Real-time 6-DoF Pose Estimation by Event-based Camera using Active LED Markers

Anonymous WACV Applications Track submission

Paper ID 282

Abstract

Real-time applications for autonomous operations depend largely on fast and robust vision-based localization systems. Since image processing tasks require processing large amounts of data, the computational resources for this task often limit the performance of other processes. To overcome this limitation, traditional marker-based localization systems are widely used since they are easy to integrate and achieve reliable accuracy. However, classical marker-based localization systems significantly depend on standard cameras with low frame rates, which often lack accuracy due to motion blur. In contrast, event-based cameras provide high temporal resolution and a high dynamic range, which can be utilized for fast localization tasks, even under challenging visual conditions. This paper proposes a simple but effective event-based pose estimation system using active LED markers (ALM) for fast and accurate pose estimation. The proposed algorithm is able to operate in real time with a latency below $0.5\,\mathrm{ms}$ *while maintaining output rates of* $3\,\mathrm{kHz}$*. Experimental results in static and dynamic scenarios are presented to demonstrate the performance of the proposed approach in terms of computational speed and absolute accuracy, using the OptiTrack system as the basis for measurement. Moreover, we demonstrate the feasibility of the proposed approach by deploying the hardware, i.e., the event-based camera and ALM, and the software in a real quadcopter application. Our project page is available at: almpose.github.io*

1. Introduction

Fast and reliable spatial localization is essential in a wide range of robotic applications. For example, in collaborative scenarios, the ability to accurately and rapidly estimate the pose of the end effector is a key component for achieving the safe, reliable and robust execution of corresponding tasks. Vision-based methods [2, 12, 36] are the most common approaches for obtaining the relative localization of objects within the line of sight. These methods achieve significantly better accuracy compared to other non-contact localization methods, *e.g.* radio-based localization approaches [10, 32]. Vision-based approaches are, however, computationally expensive and typically require more than one sensor, *e.g.* infrared-based systems [25]. To reduce the computational overhead, classical markers [13, 35] which serve as easy-to-detect anchors, are often integrated into vision-based systems. Since conventional RGB-D cameras are often used in these systems, the latency of detection cannot be reduced beyond the limit which is determined by the frame rate of the utilized cameras.

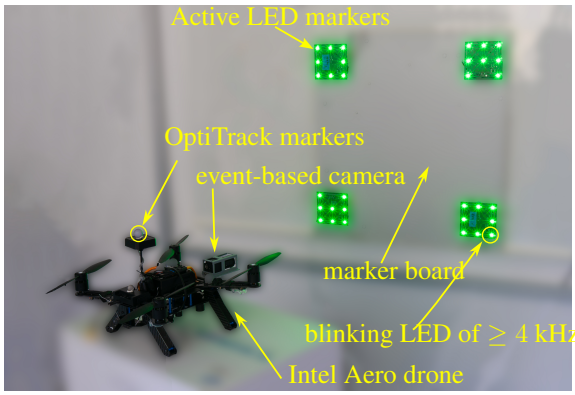

Figure 1. Overview of the experimental setup. Active LED markers (ALM) are attached to a marker board. An event-based camera mounted on a drone is used to estimate the pose of the marker board with respect to the event-based camera's frame of reference. An OptiTrack system is used for assessing the accuracy of the proposed method.

Event-based vision is an emerging field that has attracted much attention in recent years [9, 23]. Compared to conventional cameras, event-based cameras capture changes in light intensity asynchronously together with high temporal resolution and dynamic range. This feature makes them ideal for applications that require fast and accurate

*These authors contributed equally to this work.

detection. Starting from the early years of event-based vision development [8], advantages given by those sensors for robotics applications are noticable. Due to the mediocre signal-to-noise ratio and low-resolution capabilities, applications are limited and fall far behind standard RGB cameras in terms of performance. However, recent advancements in event-based sensor development [9] have enabled them to compete with the precision of other localization methods [6] due to increased resolution and reduced noise. Avoiding accumulated event representations (*i.e.* frames), markers can be tracked online utilizing the event-based camera's high temporal resolution of up to $1\,\mu s$.

In this paper, we propose a fast and simple method employing an event-based camera together with active LED markers (ALMs) for simultaneous detection and tracking of the 6 degrees-of-freedom (DoF) pose of a rigid object in the 3D space. An overview of our proposed approach is depicted in Fig. 1 with four ALMs attached to a marker board. The event-based camera is mounted on the drone, which is utilized to estimate the pose of the marker board with respect to the camera's base frame. To estimate the pose, the blinkings of the ALM's LEDs are logged with an event-based camera to identify the corresponding frequencies of each LED in the ALM. These blinking frequencies are utilized to identify each individual LED and match it with the known geometry of the ALM. With this mapping of the individual points on the camera's sensor plane and the known geometry of the ALM, the pose of the ALM can be computed by utilizing a Perspective-n-Point (PnP) algorithm. In the presented approach, by tuning the biases, i.e., parameters for tuning the analog front-end of the event-based camera, and using a priori knowledge about timing, the complexity of the ALM tracking can be simplified. This aids in reducing the tracking latency. During the tracking, the initial detection is continuously refined, resulting in subpixel resolution. Such an approach can still precisely estimate the pose even under fast rotational and linear motion. Note that the output rate is independent of the tracking performance and is limited only by the Perspective-n-Point (PnP) algorithm [17] performance. Furthermore, the proposed approach allows simultaneous tracking of multiple markers and is computationally undemanding, allowing it to be run on a wide range of devices. The proposed approach was tested and verified extensively using an external infrared-based positioning system. Our contributions are listed in the following.

- We propose the fast event-based pose estimation system using ALM achieving a latency below $0.5\,\mathrm{ms}$ while maintaining an output rate of 3 kHz.
- We analyze the proposed system in static and dynamic scenarios for several in-depth aspects, e.g., absolute accuracy, static noise, and latency. Translational error of $34.5\,\mathrm{mm} \pm 16\,\mathrm{mm}$ and $0.74° \pm 0.15°$ orientation error at distances of $2.1\,\mathrm{m}$ to $4.8\,\mathrm{m}$ between camera and marker, were achieved. Together with the fast computing speed, this proves that the proposed algorithm is promising for real-time applications.
- We integrate the proposed system into a quadcopter application for the 6-DoF pose estimation task. For indoor experiments, the proposed system outperforms the ORB-SLAM algorithm. Furthermore, in outdoor experiments, the proposed system can simultaneously detect and track the ALM in very aggressive flights at velocities of up to $10\,\mathrm{m\,s^{-1}}$.

The paper is organized as follows. Section 2 presents the related work in the field of pose estimation with event-based cameras and active markers. Section 3 describes the proposed method for marker detection and tracking. In Section 4, we present the experimental setup and results. Finally, we conclude the paper in Section 5 with a summary of our contributions and suggestions for future work.

2. Related Work

Visual localization systems show improved accuracy compared to systems based on other physical principles [26], [6]. Fiducial marker-based systems [11] constitute the most common choice for robotic applications. Due to the limited range and the dependence on the lighting conditions, some studies proposed LED-based solutions based on standard RGB cameras [34], infrared [33], or ultraviolet [30] spectrum. The pose can be retrieved much faster and more accurately due to the easy-to-extract anchor points visible in the image. However, the latency cannot be reduced beyond the camera's frame rate. This limitation can be avoided by using event-based cameras with their intrinsic high temporal resolution.

One of the first works in the direction of localization based on event-based sensors was the 2D localization method [31]. The known shape (contours) was tracked and the relative localization was determined by event-based vision. The high temporal resolution of the event-based sensors was used in [20] to localize an Unmanned Aerial Vehicle (UAV) during high-speed maneuvers. The full pose information was retrieved using a black square as a known shape. In [14] a visual odometry method was proposed based on the feature tracking algorithm. In this direction multiple methods were developed [14], [19], which show a significant improvement compared to the RGB-based approach for high-speed applications.

The utilization of ALMs was proposed first in [21], where the authors tracked the 2D position of the LED and used it as a feedback signal for the robot homing and a pan-tilt system. Later, the first method for full pose estimation using ALMs was presented in [3]. Therein, ALMs were

used to detect and estimate the position of a flying quadrocopter. Taking advantage of the high temporal resolution of the camera, LEDs were recognized and detected using event polarity changes in the event stream. In [3], the authors used an accumulated event representation to decode the frequency and estimate the pose. In [5], a Gaussian mixture probability hypothesis density filter was proposed to localize the camera with respect to the active marker. Therein, the idea of online tracking was presented to increase the robustness and reliability of the pose estimation. The achieved results indicate a localization error lower than $3\,\mathrm{cm}$ in scenarios where the camera was within $1\,\mathrm{m}$ relative to the active marker. It shall moreover be noted that in [5] standard deviation or mean values are not reported.

Most recent works using ALMs propose the additional fusion of inertial measurements [27]. The error in the predicted relative position is in the subcentimeter range. However, utilizing only the vision-based approach increases the error by the order of one magnitude. Compared to previous methods, the marker size is significantly larger. The LEDs are placed $1\,\mathrm{m}$ apart. Current work in the field of active marker-based solutions also focuses on the visual communication aspect of modulated light.

Different from other approaches in the literature, in the proposed approach, the complexity can be simplified by tuning the biases and using a priori knowledge about timing. This helps to reduce the tracking latency. To the best of the authors' knowledge, this work achieves the lowest latency compared to other methods in the literature. During tracking, initial detection is continuously refined, resulting in subpixel resolution. Such an approach can still precisely estimate the pose even under fast rotational and linear motion. The output rate is independent of the tracking performance and is limited only by the Perspective-n-Point (PnP) algorithm [17]. The method allows simultaneous tracking of multiple markers and is computationally undemanding, allowing it to be run on a wide range of devices. The proposed approach was tested and verified extensively using an external infrared-based positioning system.

3. Active Marker Tracking and Pose Estimation

An event-based camera consists of an array of independent pixels measuring changes in luminosity $L = \log(I)$, based on the photocurrent I [16]. A change in the continuous luminosity signal

$$\Delta L(\mathbf{u}_k, t_k) = L(\mathbf{u}_k, t_k) - L(\mathbf{u}_k, t_k - \Delta t_k) > p_k C \quad (1)$$

triggers an event $\mathbf{e}_k = (\mathbf{u}_k, t_k, p_k)$ at pixel location $\mathbf{u}_k = (u_k, v_k)$ due to a temporal contrast threshold $\pm C$, $p_k \in \{+1, -1\}$ being its polarity and Δt_k its time since the last event (at $\mathbf{u}_k$) occurred at t_k [9]. The current generation of event-based sensors can produce up to 1.2 Giga events per second (Geps) [9] with a microsecond range timestamp accuracy. Compared to frame-based cameras that deliver periodically dense (*i.e.* full-frame) information, the event stream is sparse and contains information that relates only to changes in the scene. Using ALMs, the periodic and dense signals can be generated as a projection of the LED on the camera's sensor plane.

To reduce the computational complexity and required bandwidth, the biases of the sensor are tuned to generate a single event per pixel on every LED blink while suppressing all other background events to increase the signal-to-noise ratio, as presented in Figure 2. While [3] uses events of both polarities and relatively low frequencies (1-2kHz), the amount of noise can be reduced by using higher frequencies and disabling one polarity.

The ALM's structure is an arrangement of high-frequency blinking LEDs, where a unique frequency of the blinking pattern can individually recognize each LED (*e.g.* different blinking frequencies). The arrangement of the LEDs has to be fixed and determined in 3D coordinate space. However, it can also be arranged on a plane, as utilized in this work. Based on the 2D projection of the LEDs, knowing their 3D arrangement and camera intrinsics, the relative pose of the marker with respect to the sensor can be reconstructed using a Point-n-Perspective (PnP) algorithm [18]. In this work, the *IPPE* PnP algorithm is used [7].

The proposed approach is divided into four parts, as illustrated in Fig. 2. To reduce the noise in the signal the bias settings are tuned to produce a single event per pixel on every blink of a LED. Next, events are accumulated over a period of $\frac{2}{f_{\min}}$ and for the accumulated event clusters, frequencies are recognized. These frequencies are used to identify newly appearing ALMs. For each of the ALM's LEDs, trackers are spawned that keep track of the LEDs' center points based on single events. The tracking of the LEDs is independent of the detection loop. The pose of the ALM is estimated utilizing the trackers of the ALM. The accuracy of the pose estimation can be obtained using the reprojection error. When an ALM leaves the field of view or the reprojection error exceeds the defined maximal value, the corresponding trackers are deleted. If the ALM enters the field of view again, the detection respawns it. Such a two-folded approach reduces latency and increases the accuracy of the solution.

3.1. Detection

The detection of an ALM includes the recognition of an individual ALM and the estimation of the blinking frequencies for each LED. For this, the geometrical arrangement, as well as the blinking frequency of the ALM LEDs, has to be provided a priori.

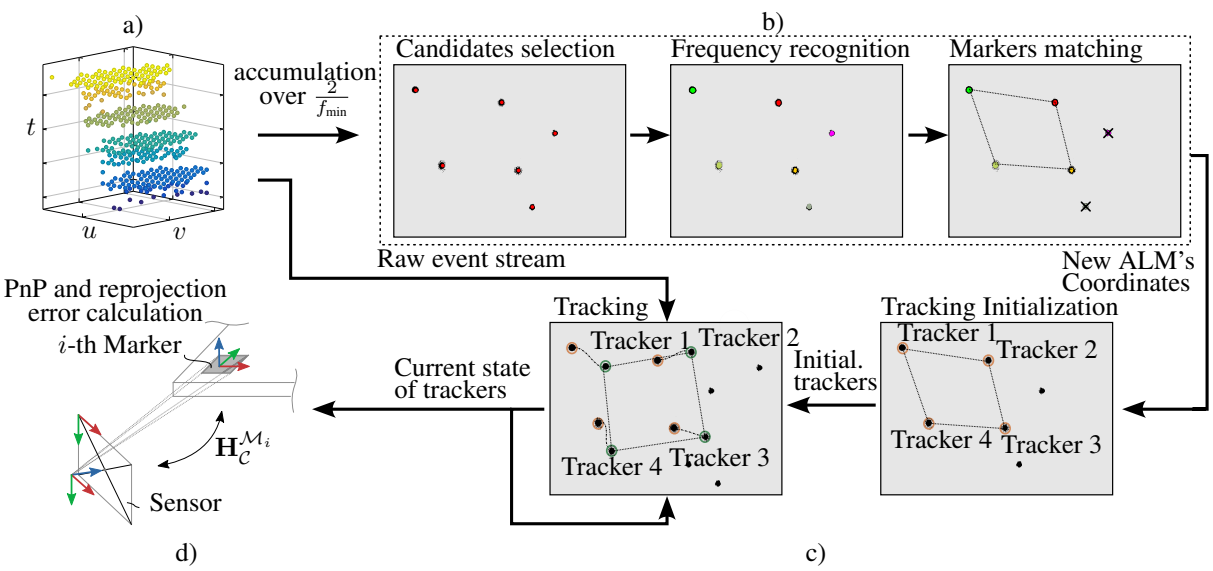

Figure 2. Overview of the proposed approach. Our pipeline consists of four asynchronous parts. *First*, illustrated in (a), to reduce the noise in the signal, biases are tuned to produce a single event per pixel on every blink. The proposed detection algorithm accumulates the events over a short period of time (two times the period of the minimal frequency LED to ensure at least two blinks are visible for every LED). *Second*, for the accumulated blinks, frequencies are recognized and assigned to the specified markers. For every detected marker (b), trackers (c) are spawned for each individual LED. *Third*, using a simple tracking procedure, the LEDs are being tracked independently. *Fourth*, to quantify tracking quality during runtime, the resulting solution (d) is used to compute the reprojection errors.

The range of possible frequencies for the LEDs is wide: from tests conducted, frequencies higher than 4kHz and lower than 40kHz work best. To detect lower frequencies, biases have to be adapted to maximize the signal-to-noise ratio. As the timestamp is quantized, it is advisable to use LED frequencies with an integer microsecond period.

Due to the limited noise, detection can be simplified by using only single types of events. While in [27] and [3], the detections rely on the transitions between event polarities. Instead, in the proposed approach, we rely only on the timing information between consecutive events generated by a single pixel.

For detection, an event frame generated over the period T_d is used. T_d has to be larger than $\frac{2}{f_{\min}}$ of the minimal used frequency $f_{\min}$ (typ. $f_{\min} \approx 2\,\mathrm{kHz}$) to ensure that at least two blinks are visible for every LED. Candidates for the blinking LEDs can be retrieved by selecting the connected regions where more than $T_d f_{\min}$ events per pixel are generated. Each region with an area larger than a defined minimal area is selected as a potential candidate. Due to the short accumulation period, even under fast motion, the LEDs' center points can be calculated by computation of the center of mass on a 2D plane. The error introduced by the relative movement of the LED is refined by the tracking procedure.

For the frequency estimation of the LEDs, a histogram of the time differences between events in a given area is used. In the case of frequencies with an integer microsecond period, the histogram has a pronounced peak, while for other frequencies, the histogram follows a wider Gaussian distribution. The frequency estimation follows the procedure proposed in [3].

3.2. Tracking

While detection relies on an accumulated representation of the events, the tracking can be performed online to reduce latency. Using the initial guess from the detection of the ALM's LED center points, trackers are spawned for every LED. The i-th tracker is characterized by its frequency f_i, center point $\mathbf{c}_i = [x_i, y_i]$ and radius r_i. In comparison to the assumptions of [15] and [24], the distribution of the generated events (within one blink) follows a spatially uniform distribution and hence, produces a dense event stream in this region. This allows us to simplify the tracking algorithm while maintaining precise tracking with sub-pixel accuracy.

For every LED's blink, the tracker's center of mass $\bar{\mathbf{c}}_i$ is calculated using all events within its current radius r_i. The update term

$$\bar{\mathbf{c}}_i = \tilde{\beta}\mathbf{u}_k + (1-\tilde{\beta})\bar{\mathbf{c}}_i\,, \tag{2}$$

introduces low-pass filtering, where every new event $\mathbf{u}_k$ updates the current solution directly with an update factor $\tilde{\beta}$ of typically 0.02. The radius r_i is updated every N events and set to twice the average distance of the events with respect to the center point of the tracker.

3.3. Pose Estimation

The 6-DoF pose is estimated asynchronously, using the current center points of the ALM's trackers. To increase the update rate of the algorithm, a PnP algorithm is started whenever the previous iteration is done. Due to the simplicity of the tracking, the PnP calculation is decisive in terms of latency and output rate.

To ensure stability and detect tracking failures, the reprojection error is computed and compared to the tracker's center points. When the reprojection error of one tracker exceeds the mean distance of the events from the center point, a tracking lost signal is generated, and tracking is stopped. It is reinitialized with the first new detection of a given marker.

4. Experiments

4.1. Setup

For the experimental setup, the EVK4 HD evaluation kit from Prophesee is used. It includes the event-based vision sensor IMX636ES providing HD resolution (1280×720 pixels) and the Soyo SFA0820-5M lens. The ALM consists of printed circuit boards with 8 LEDs arranged in a square of $9\,\mathrm{cm}$ side length. Each ALM has a base frequency (first LED), and the remaining frequencies are selected to match integer microsecond period times. For the experiments, four markers are arranged in a square resulting in a marker board with a side length of $59\,\mathrm{cm}$. From this, 8 outermost LEDs were chosen to create a single marker. The camera's bias settings are set to minimize noise while maintaining a high event rate caused by the ALMs. The processing of the event stream is done on a PC running Ubuntu 20.04 with an Intel i9-12900K processor and 32GB of RAM and Intel Aero Compute Board. The camera is connected via USB 3 and the camera's external trigger input is used for time synchronization between the PC and the camera. As ground truth, the commercial infrared 3D tracking system OptiTrack is used, comprising nine Prime 17W cameras. The OptiTrack recordings are triggered with the same external trigger signal as the event-based camera. In order to use the event-based camera simultaneously with the OptiTrack system, an infrared filter is used.

4.2. Bias Adjustment

The bias adjustment of the event camera is essential for the proposed system's performance. The IMX636ES sensor biases [1] allow control over analog pixel gate thresholds to achieve the desired sensor response. The adjustment goal is to minimize the number of activated pixels between two LED blinks, thereby reducing processing complexity. The proposed method employs a single event polarity for simplicity.

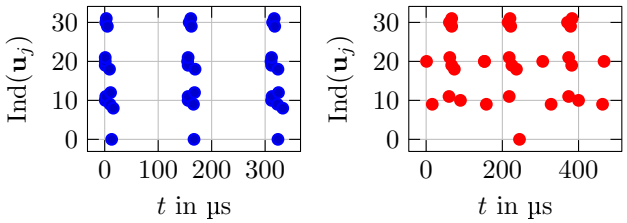

(a) Adjusted biases (b) Default biases

Figure 3. Visualization of bias adjustment in an event camera using the IMX636ES sensor. The vertical axis represents the flattened indices of the pixels in the region of interest (ROI) around an LED light. The left plot demonstrates an optimal bias adjustment, where event fronts - closely packed clusters of events triggered by a rapid change in the scene (like a sudden LED blink) - are clearly distinct. No unwanted spurious events occur between these event fronts. The right plot, in contrast, displays the event distribution with the camera's default bias settings, showing a less distinct separation of event fronts.

By adjusting the refractory period setting, a pixel should be rendered insensitive to subsequent changes in LED brightness. An optimal value during adjustments should filter out all events between two consecutive LED-triggered events. By utilizing high-pass and low-pass filter setups, the number of environment-generated events (excluding those by LEDs) can be limited to prevent sensor overflow and maintain manageable event blob density, as shown in Figure Fig. 3.

A detailed explanation of sensor biases is provided in [1]. The description of the bias adjustment procedure is given in our supplementary document. Although the focus here is on the IMX636ES sensor, the setup procedure should be applicable to cameras from other manufacturers.

4.3. Absolute Accuracy

To evaluate the absolute accuracy, the pose estimation of the ALMs and the marker board are compared with the synchronized measurements of the OptiTrack system (ground truth). For this experiment, the marker board is placed statically in the scene. The camera moves from close to far, covering the working distance of the setup, which is limited by the OptiTrack setup. The kinematic relations of the experimental setup are described in detail in the appendix.

The magnitude of the absolute position error $\mathbf{e}_t$ and the orientation error Θ_r with the distance between the marker and the camera $\left\|\mathbf{d}_{\mathcal{C}}^{\mathcal{M}}\right\|$, ranging from $2.1\,\mathrm{m}$ to $4.8\,\mathrm{m}$, as well as the orientation $\mathbf{\Theta}_{\mathcal{C}}^{\mathcal{M}}$ of the marker with respect to the camera, is depicted in Fig. 4. The difference of using a single ALM with a side length of $9\,\mathrm{cm}$ for pose estimation compared to a larger marker board with a side length of $59\,\mathrm{cm}$ is illustrated. The plot of the position error $\|\mathbf{e}_t\|$ in Fig. 4 shows less noise but comparable error magnitude.

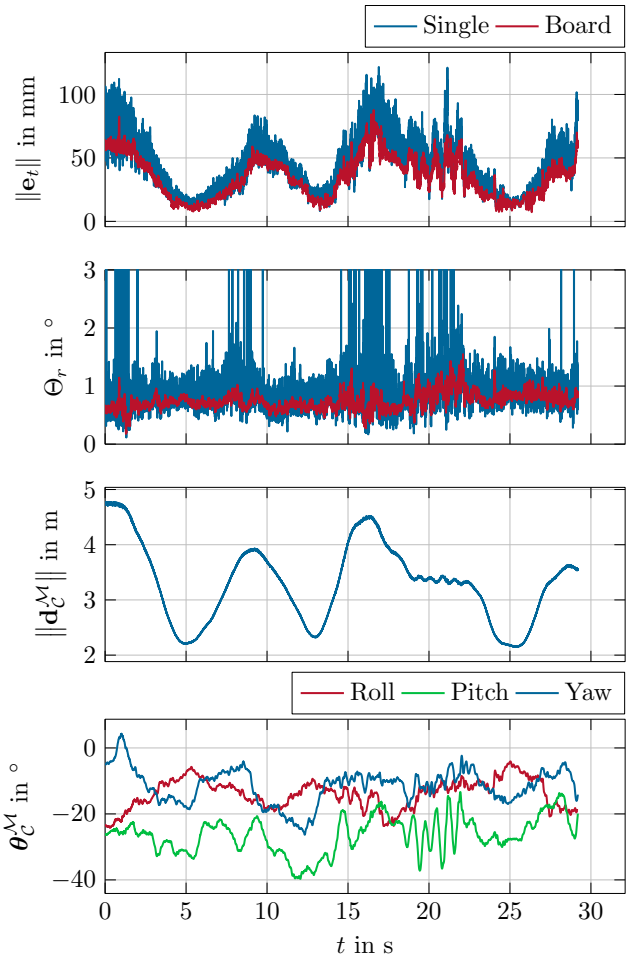

Figure 4. The ALM and the marker board are placed statically in the scene, and the camera moves from close to far. The first plot shows the absolute translational error of a single ALM and the whole marker board. The second plot displays the orientation error, with the third and fourth plot indicating the distance $\|\mathbf{d}_C^{\mathcal{M}}\|$ ($\min\|\mathbf{d}\|_C^{\mathcal{M}} = 2.1\,\mathrm{m}$, $\max\|\mathbf{d}\|_C^{\mathcal{M}} = 4.8\,\mathrm{m}$) and the orientation $\boldsymbol{\Theta}_C^{\mathcal{M}}$ between the camera and the marker.

The second plot displaying the orientation error Θ_r shows significant spikes for the single ALM curve. This indicates flips in the estimated pose, especially for medium to far distances. Hence, the usage of a marker board with increased side length is beneficial for accurate orientation estimations. The plot of the marker orientation $\boldsymbol{\Theta}_C^{\mathcal{M}}$ in Fig. 4 shows fast orientation changes beginning at 20 s. This demonstrates the ability of the proposed method to estimate pose information even in highly dynamic scenes accurately.

In order to compare the performance between the detection-based pose estimation (Sec. 3.1) and the tracking-based pose estimation (Sec. 3.2) the relative position error $\tilde{e}_t = \frac{\|\mathbf{e}_t\|}{\|\mathbf{d}_C^{\mathcal{M}}\|}$ is displayed in Fig. 5 with respect to the

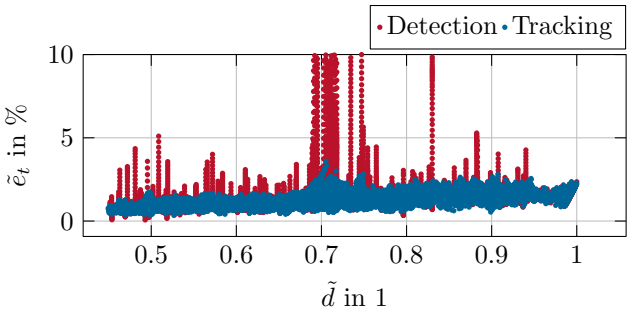

Figure 5. Comparison between the detection and tracking algorithm for pose estimation. The relative position error $\tilde{e}_t$ is plotted over the normalized distance $\tilde{d}$.

normalized distance $\tilde{d} = \frac{\|\mathbf{d}\|_C^{\mathcal{M}}}{\max\|\mathbf{d}\|_C^{\mathcal{M}}}$. The results for the tracking-based approach indicate a better consistency, *i.e.* less noise, and altogether lower error numbers in the 1 % to 2 % range. The expected linear increase of the position error with distance is displayed as well.

The statistical values of the data illustrated in Fig. 5 are summarized in Tab. 1. The maximum position error of 87.8 mm at a distance of 4.8 m and the maximum orientation error of 1.55° indicate the excellent performance of the tracking-based approach. The standard deviation of the position and orientation error of 16.2 mm and 0.146°, respectively, indicate the robustness of our method.

Table 1. Statistical values of the absolute accuracy measurements for the detection-based and the tracking-based approach.

	Tracking		Detection	
	$\|\mathbf{e}_t\|$	Θ_r	$\|\mathbf{e}_t\|$	Θ_r
Mean	34.5 mm	0.738°	64.9 mm	1.55°
Std. Dev.	16.2 mm	0.146°	121 mm	5.12°
Maximum	87.8 mm	1.55°	1.233 m	71.9°

4.4. Static Noise

In Tab. 2, the noise floor of the proposed method is characterized at different distances between the camera and the marker board. The low standard deviation values indicate the stability of the pose estimation. This data can be utilized to tune Bayesian filters (*e.g.* Kalman filters) in the subsequent data processing in applications.

Table 2. Statistics of the noise in static scenes at different distances between marker and camera.

$\|\mathbf{d}_C^{\mathcal{M}}\|$	Std. Dev.	Maximum
6 m	1.4 mm	5.5 mm
4 m	0.68 mm	2.95 mm
2 m	0.25 mm	2.17 mm

4.5. Latency Measurement and Output Rate

To determine the latency of the proposed system, the execution priority was elevated. Additionally, the visualization, as well as background tasks of the operating system, were disabled. This avoids unintentional interrupts and stalls during the execution of the pose estimation.

The latency and output rate values are listed in Tab. 3 and Tab. 4. The output rate of the tracking-based approach outperforms the detection-based method while achieving comparable latency results. As shown in Table Tab. 4, the proposed method is capable of running even on an embedded PC with an Intel Atom processor on an Intel Aero Ready to Fly Drone. While maintaining real-time performance, we can notice a reduced output rate (limited by the PnP computation time) as well as an increased average delay (limited by a number of concurrent threads) compared to a desktop PC. Latency is measured using a precise synchronization trigger signal and is equal to the time difference between the trigger and the time when pose estimation for this timestamp is available.

Our proposed method achieves lower mean latency combined with low standard deviation compared to the state-of-the-art. To further reduce the latency it is possible to implement this solution on different hardware architectures, *e.g.* FPGAs. A large part of the resulting latency is due to communication overhead.

Table 3. Latency and output rates for the detection-based and the tracking-based approach. (Desktop PC)

	Tracking		Detection	
	latency	rate	latency	rate
Mean	354 µs	3.805 kHz	699 µs	0.670 kHz
Std. Dev.	92 µs	0.064 kHz	35 µs	0.288 kHz

Table 4. Latency and output rates for the detection-based and the tracking-based approach. (Intel Aero Compute Board)

	Tracking		Detection	
	latency	rate	latency	rate
Mean	1232 µs	1.32 kHz	1953 µs	0.223 kHz
Std. Dev.	194 µs	0.14 kHz	240 µs	0.094 kHz

4.6. Application to 6-DoF position estimation for a quadcopter

In this section, indoor and aggressive outdoor flights are considered for 6-DoF position estimation of a quadcopter.

4.6.1 Indoor flight experiments

Compared to stationary robots, e.g. articulated manipulators [28, 29], which are equipped with high-precision encoders to monitor their state, flying robots mainly rely on IMUs, barometers, and vision-based systems to estimate their state. While the pose estimation module equipped with only IMUs and barometers often suffers from the problem of drift, vision-based systems ensure a more reliable measurement. In this experiment, the Intel® Aero Ready to Fly (RTF) Drone, shown in Fig. 1, is employed as it offers enough computational power for on-board processing of all algorithms.

For absolute drift-free pose information, the ORB-SLAM2 [22] algorithm is utilized. The ORB-SLAM2 was chosen for its impressive performance and open-source implementation. Note that ORB-SLAM3 [2], as the successor of ORB-SLAM2, is a more robust version compared to ORB-SLAM2. However, the accuracy of these approaches on stereo and RGB-D cameras is still comparable since the key concepts of the estimation module and the relocalization method, remain unchanged. We are aware that comparing the proposed system with other SLAM algorithms, e.g., feature-based SLAM [22] and event-based SLAM [4], may not be a fair comparison because the key concept is different. However, this comparison could provide a qualitative guide for choosing the right methods in a given situation and contextualize results. Similar to previous subsections, the OptiTrack serves as the source of ground truth.

For the translational errors, the metric for comparison is the difference between a ground truth position and the estimated position as $\mathbf{p}_e = [p_{e,x}\ p_{e,y}\ p_{e,z}]^{\mathrm{T}} = \mathbf{p}_g - \hat{\mathbf{p}}$, where the hat $(\hat{\cdot})$ indicates quantities estimated by the ORB-SLAM2 algorithm [22] or with the event-based marker, respectively, the subindex $(\cdot)_g$ stands for the three-dimensional ground truth quantities, and the subindex $(\cdot)_e$ for the resulting three-dimensional errors. The orientation errors are represented in Euler angles. The difference between the ground truth quaternion and the estimated quaternion is defined as $\mathbf{q}_e = \hat{\mathbf{q}}^{-1} \otimes \mathbf{q}_g$ with $\otimes$ is the quaternion product. Subsequently, this error quaternion can be transformed into an equivalent representation using three angles, i.e., roll, pitch, and yaw. In this experiment, the quadcopter is moved aggressively in a zigzag pattern in a space of $1.8\,\mathrm{m}$ in the x-direction, $0.6\,\mathrm{m}$ in y-direction, and $0.4\,\mathrm{m}$ in z-direction for about $50\,\mathrm{s}$. The position estimates and the resulting errors for this case are illustrated in Fig. 6 and Fig. 7. The errors obtained from the proposed algorithm in the x-, y- and z-direction are bounded within $\pm 0.06\,\mathrm{m}$, $\pm 0.08\,\mathrm{m}$, and $\pm 0.02\,\mathrm{m}$, respectively, while larger errors result from the ORB SLAM, i.e., $p_{e,x} = \pm 0.2\,\mathrm{m}$, $p_{e,y} \in [-0.2, 0.1]^{\mathrm{T}}\,\mathrm{m}$, and $p_{e,z} = \pm 0.05\,\mathrm{m}$. The orientation errors achieved with the two methods are similar, shown at the bottom of Fig. 7. However, the orientation errors measured by the proposed system are slightly better since the spikes in ORB SLAM are larger. More experiments can be found in our supplementary material.

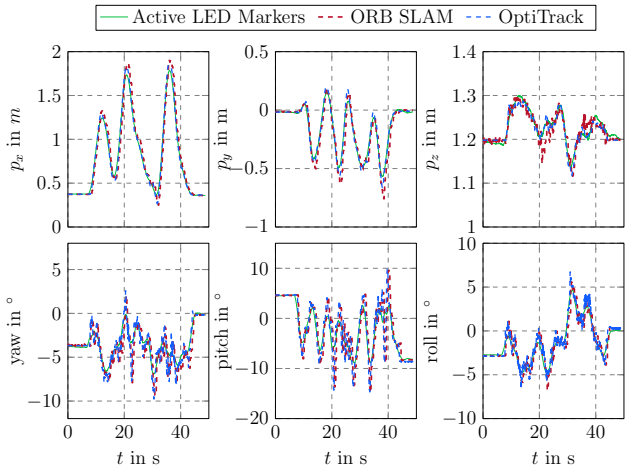

Figure 6. Time evolution of the drone trajectory. The estimated poses from the proposed method, the ORB SLAM, and the ground truths from OptiTrack are illustrated in green, red, and blue, respectively.

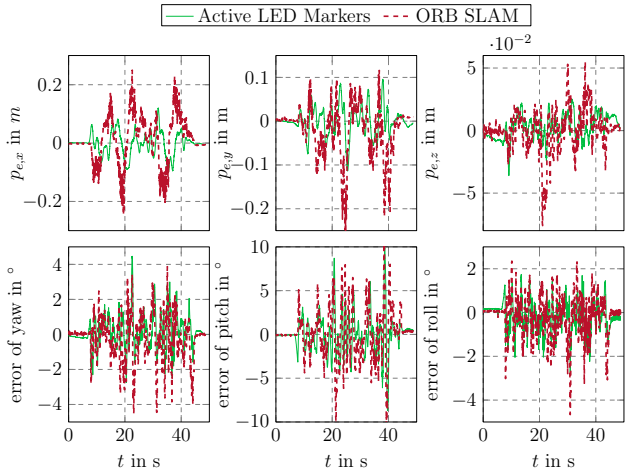

Figure 7. The error plots of the corresponding estimates, depicted in Fig. 6 with respect to the ground truth measurements from the OptiTrack.

4.6.2 Outdoor Flight Experiments

Outdoor experiments were conducted to demonstrate the capability of the proposed system to detect and track motions at very high speeds. In the first scenario, the drone is equipped with an ALM and the event-based camera is mounted vertically on the tripod on the ground, see the left-hand side of Fig. 8a. Although the drone moves at a maximum speed of $4.5\,\mathrm{m\,s^{-1}}$ and ascends to a height of $9\,\mathrm{m}$, the proposed system is still able to capture the trajectories of the ALM, depicted on the right-hand side of Fig. 8b. The position signals $\mathbf{d}_C^{\mathcal{M}}$ indicate a low noise floor. The velocity signals $\dot{\mathbf{d}}_C^{\mathcal{M}}$ are calculated based on the position signals with

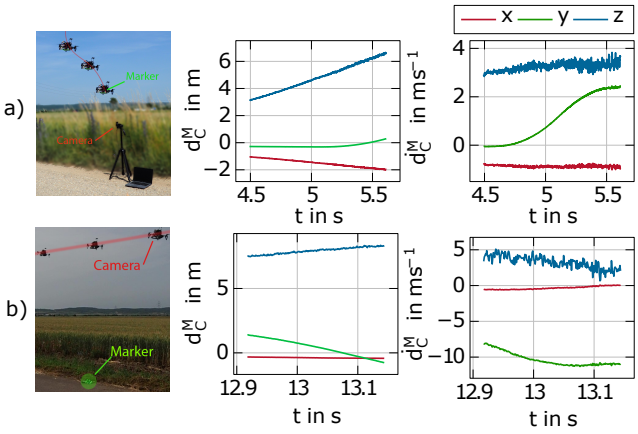

Figure 8. The plot of the drone's trajectory during experimets. a) Camera on ground b) Camera mounted on the drone. The left plot illustrates the position with the corresponding velocity shown in the right plot. The derivative of the positional signal was filtered with a moving average filter with a window length of 100 samples to obtain the plotted velocity signal.

additional moving average filtering. Unlike in the first scenario, the camera is mounted on the drone, and the ALM is static on the ground in the second scenario, as illustrated on the left-hand side of Fig. 8b. The captured trajectories are shown on the right side of Fig. 8b when the drone is moving with an average speed of $10\,\mathrm{m\,s^{-1}}$. In both scenarios, the velocity in the z direction is noisy due to the higher noise in the z estimation by the PnP algorithm. Live videos of the two scenarios are provided in the supplemental material.

5. Conclusion

This paper presents a fast and accurate vision-based localization system using an event-based camera with active led markers. Our proposed method overcomes the limits of traditional marker-based localization systems, *i.e.* low frame rate, motion blur, and high computational costs, by utilizing the advantages of an event-based camera. The proposed algorithm is simple but effective, achieving real-time performance with minimal latency below $0.5\,\mathrm{ms}$ and output rates above $3\,\mathrm{kHz}$ using a regular PC. The proposed tracking-based approach outperforms detection-based methods, especially in applications with very fast movements. the position error normalized to the distance is constantly below $1.87\,\%$ with a mean orientation error of $0.738°$. To the best of the authors' knowledge, the combination of the achieved precision at this output rate and latency was not achieved so far. The proposed method opens new possibilities for robotic applications where the high output rates and high precision of 6-DoF pose estimation are important, *e.g.* dynamic handover tasks and pick-and-place tasks.

References

[1] Biases — metavision SDK docs 4.1.0 documentation. 5

[2] Carlos Campos, Richard Elvira, Juan J Gómez Rodríguez, José MM Montiel, and Juan D Tardós. Orb-slam3: An accurate open-source library for visual, visual–inertial, and multimap slam. *IEEE Transactions on Robotics*, 37(6):1874–1890, 2021. 1, 7

[3] Andrea Censi, Jonas Strubel, Christian Brandli, Tobi Delbruck, and Davide Scaramuzza. Low-latency localization by active LED markers tracking using a dynamic vision sensor. In *IEEE/RSJ International Conference on Intelligent Robots and Systems*, pages 891–898, 2013. 2, 3, 4

[4] William Chamorro, Joan Solà, and Juan Andrade-Cetto. Event-based line slam in real-time. *IEEE Robotics and Automation Letters*, 7(3):8146–8153, 2022. 7

[5] Guang Chen, Wenkai Chen, Qianyi Yang, Zhongcong Xu, Longyu Yang, Jörg Conradt, and Alois Knoll. A novel visible light positioning system with event-based neuromorphic vision sensor. *IEEE Sensors Journal*, 20(17):10211–10219, 2020. 3

[6] Siyuan Chen, Dong Yin, and Yifeng Niu. A Survey of Robot Swarms' Relative Localization Method. *Sensors*, 22(12):4424, 2022. 2

[7] Toby Collins and Adrien Bartoli. Infinitesimal plane-based pose estimation. 109(3):252–286. 3

[8] Tobi Delbruck and Manuel Lang. Robotic goalie with 3 ms reaction time at 4event-based dynamic vision sensor. *Frontiers in Neuroscience*, 7:223, 2013. 2

[9] Guillermo Gallego, Tobi Delbruck, Garrick Orchard, Chiara Bartolozzi, Brian Taba, Andrea Censi, Stefan Leutenegger, Andrew J. Davison, Jorg Conradt, Kostas Daniilidis, and Davide Scaramuzza. Event-Based Vision: A Survey. *IEEE Transactions on Pattern Analysis and Machine Intelligence*, 44(1):154–180, 2022. 1, 2, 3

[10] Milad Heydariaan, Hessam Mohammadmoradi, and Omprakash Gnawali. Toward standard non-line-of-sight benchmarking of ultra-wideband radio-based localization. In *IEEE Workshop on Benchmarking Cyber-Physical Networks and Systems*, pages 19–24, 2018. 1

[11] Michail Kalaitzakis, Brennan Cain, Sabrina Carroll, Anand Ambrosi, Camden Whitehead, and Nikolaos Vitzilaios. Fiducial markers for pose estimation. *Journal of Intelligent & Robotic Systems*, 101(4):71, 2021. 2

[12] Iman Abaspur Kazerouni, Luke Fitzgerald, Gerard Dooly, and Daniel Toal. A survey of state-of-the-art on visual slam. *Expert Systems with Applications*, 205:117734, 2022. 1

[13] Oguz Kedilioglu, Tomás Marcelo Bocco, Martin Landesberger, Alessandro Rizzo, and Jörg Franke. Arucoe: Enhanced aruco marker. In *International Conference on Control, Automation and Systems*, pages 878–881, 2021. 1

[14] Beat Kueng, Elias Mueggler, Guillermo Gallego, and Davide Scaramuzza. Low-latency visual odometry using event-based feature tracks. In *IEEE/RSJ International Conference on Intelligent Robots and Systems*, pages 16–23, 2016. 2

[15] Xavier Lagorce, Cédric Meyer, Sio-Hoi Ieng, David Filliat, and Ryad Benosman. Asynchronous event-based multikernel algorithm for high-speed visual features tracking. *IEEE Transactions on Neural Networks and Learning Systems*, 26(8):1710–1720, 2015. 4

[16] Patrick Lichtsteiner, Christoph Posch, and Tobi Delbruck. A 128×128 120 dB 15μs Latency Asynchronous Temporal Contrast Vision Sensor. *IEEE Journal of Solid-State Circuits*, 43(2):566–576, 2008. 3

[17] Xiao Xin Lu. A review of solutions for perspective-n-point problem in camera pose estimation. In *Journal of Physics: Conference Series*, volume 1087, page 052009, 2018. 2, 3

[18] K. Madsen, H.B. Nielsen, O. Tingleff, and Danmarks tekniske universitet. Informatik og Matematisk Modellering. *Methods for Non-linear Least Squares Problems*. Informatics and Mathematical Modelling, Technical University of Denmark, 2004. 3

[19] Elias Mueggler, Guillermo Gallego, Henri Rebecq, and Davide Scaramuzza. Continuous-time visual-inertial odometry for event cameras. *IEEE Transactions on Robotics*, 34(6):1425–1440, 2018. 2

[20] Elias Mueggler, Basil Huber, and Davide Scaramuzza. Event-based, 6-DOF pose tracking for high-speed maneuvers. In *IEEE/RSJ International Conference on Intelligent Robots and Systems*, pages 2761–2768, 2014. 2

[21] Georg R. Muller and Jorg Conradt. A miniature low-power sensor system for real time 2D visual tracking of LED markers. In *IEEE International Conference on Robotics and Biomimetics*, pages 2429–2434, 2011. 2

[22] Raul Mur-Artal and Juan D Tardós. Orb-slam2: An open-source slam system for monocular, stereo, and rgb-d cameras. *IEEE Transactions on Robotics*, 33(5):1255–1262, 2017. 7

[23] Anh Nguyen, Thanh-Toan Do, Darwin G. Caldwell, and Nikos G. Tsagarakis. Real-time 6dof pose relocalization for event cameras with stacked spatial lstm networks. In *IEEE/CVF Conference on Computer Vision and Pattern Recognition Workshops*, pages 1638–1645, 2019. 1

[24] David Reverter Valeiras, Xavier Lagorce, Xavier Clady, Chiara Bartolozzi, Sio-Hoi Ieng, and Ryad Benosman. An asynchronous neuromorphic event-driven visual part-based shape tracking. *IEEE Transactions on Neural Networks and Learning Systems*, 26(12):3045–3059, 2015. 4

[25] Nasir Saeed, Haewoon Nam, Tareq Y Al-Naffouri, and Mohamed-Slim Alouini. A state-of-the-art survey on multidimensional scaling-based localization techniques. *IEEE Communications Surveys & Tutorials*, 21(4):3565–3583, 2019. 1

[26] Wilson Sakpere, Michael Adeyeye Oshin, and Nhlanhla Mlitwa. A state-of-the-art survey of indoor positioning and navigation systems and technologies. *South African Computer Journal*, 29:145, 2017. 2

[27] Mohammed Salah, Mohammed Chehadah, Muhammed Humais, Mohammed Wahbah, Abdulla Ayyad, Rana Azzam, Lakmal Seneviratne, and Yahya Zweiri. A neuromorphic vision-based measurement for robust relative localization in future space exploration missions. *CoRR*, 2022. 3, 4

[28] Yvonne Stürz, Lukas Affolter, and Roy Smith. Parameter identification of the KUKA LBR iiwa robot including constraints on physical feasibility. *IFAC-PapersOnLine*, 50(1):6863–6868, 2017. 7

[29] Minh Nhat Vu, Florian Beck, Christian Hartl-Nesic, Anh Nguyen, and Andreas Kugi. Machine learning-based framework for optimally solving the analytical inverse kinematics for redundant manipulators. *Mechatronics*, 91:102970, 2023. 7

[30] Viktor Walter, Martin Saska, and Antonio Franchi. Fast Mutual Relative Localization of UAVs using Ultraviolet LED Markers. In *International Conference on Unmanned Aircraft Systems*, pages 1217–1226, 2018. 2

[31] David Weikersdorfer and Jörg Conradt. Event-based particle filtering for robot self-localization. In *IEEE International Conference on Robotics and Biomimetics*, pages 866–870, 2012. 2

[32] Henk Wymeersch, Jiguang He, Benoit Denis, Antonio Clemente, and Markku Juntti. Radio localization and mapping with reconfigurable intelligent surfaces: Challenges, opportunities, and research directions. *IEEE Vehicular Technology Magazine*, 15(4):52–61, 2020. 1

[33] Xudong Yan, Heng Deng, and Quan Quan. Active infrared coded target design and pose estimation for multiple objects. In *IEEE/RSJ International Conference on Intelligent Robots and Systems*, pages 6885–6890, 2019. 2

[34] Masaki Yoshino, Shinichiro Haruyama, and Masao Nakagawa. High-accuracy positioning system using visible led lights and image sensor. In *IEEE Radio and Wireless Symposium*, pages 439–442, 2008. 2

[35] Xiang Zhang, Stephan Fronz, and Nassir Navab. Visual marker detection and decoding in ar systems: A comparative study. In *International Symposium on Mixed and Augmented Reality*, pages 97–106, 2002. 1

[36] Yong Zhao, Shibiao Xu, Shuhui Bu, Hongkai Jiang, and Pengcheng Han. Gslam: A general slam framework and benchmark. In *IEEE/CVF International Conference on Computer Vision*, pages 1110–1120, 2019. 1